Blob Transport Models, Experiments, and the Accretion Theory of Spontaneous Rotation*

J.R. Myra 1), J. Boedo 2), B. Coppi 3), D.A. D'Ippolito 1), S.I. Krasheninnikov 2),
B.P. LeBlanc 4), M. Lontano 5), R. Maqueda 6), D.A. Russell 1), D.P. Stotler 4),
M.C. Varischetti 5), S.J. Zweben 4), and the NSTX Team.

1) Lodestar Research Corp., Boulder CO, USA;
2) UCSD, San Diego CA, USA;
3) MIT, Cambridge MA, USA;
4) PPPL, Princeton NJ, USA;
5) FP–CNR, Euratom-ENEA-CNR, Milan, Italy;
6) Nova Photonics, Princeton NJ, USA.

e-mail contact of main author: jrmyra@lodestar.com

Abstract. Radial convective transport competes with classical parallel transport to determine the radial penetration of plasma into the tokamak scrape-off-layer (SOL), influencing recycling and wall damage. This motivates theoretical models and experimental verification of blob velocity scalings discussed in this paper. In a separate study, recent developments in the "Accretion Theory" of spontaneous tokamak rotation, and its relation to blob physics are also considered.

1. Introduction

Blobs are intermittent filamentary convecting plasma structures. Models based on the "blob" paradigm provide a useful conceptual framework for transport in the scrape-off-layer (SOL) of fusion devices.

The theory of curvature-driven blob transport regimes in a tokamak is described in Sec. 2.1 and employed to make testable predictions for the magnitude and scaling of the blob radial velocity. The electrostatic theory encompasses the sheath-connected, resistive X-point and resistive-ballooning-disconnected regimes, and is therefore applicable to both X-point and limiter configurations. Gas puff imaging (GPI), a fast-time-scale high-spatial-resolution imaging technique, presents a new opportunity, investigated here, for the comparison of blob theory with 2D data. The atomic and neutral physics aspects of interpreting GPI images are studied in Sec 2.2. It is shown that the single state collisional radiative (CR) model is able to resolve time variations slower than 1 μs and is, thus, suitable for present GPI experiments. In Sec. 2.3, using GPI data from the NSTX tokamak, the blob velocity is analyzed and interpreted in terms of blob models. We find that the observed velocity is bounded by theoretically predicted minimum and maximum velocities corresponding to the sheath-connected and resistive-ballooning-disconnected limits respectively.

Finally, in a separate study, recent developments in the "accretion theory" of spontaneous tokamak rotation, and its relation to blob physics are also considered. The extensive series of recent experimental observations that are consistent with the predictions of and the interpretation by the "Accretion Theory" of the spontaneous rotation phenomenon is analyzed. Relevant developments of this theory are presented. Momentum transport from quasi-linear pinch and diffusion terms are evaluated for the ion temperature gradient (ITG) modes including velocity shear (Sec. 3.1) and the velocity gradient driven VTG modes (Sec. 3.2). The process of angular momentum ejection from the plasma column to the surrounding wall is attributed to the formation of blobs which arise from modes excited at the edge of the plasma column. Relevant modes and the nonlinear simulations of the ejection process are considered in Secs. 3.2 and 3.3.

2. Blob physics and imaging analysis

2.1 Blob Transport Regimes and Models

A filamentary structure of localized plasma (blob) in the SOL is subject to e/i charge separation from curvature and grad-B drifts. [1, 2] The resulting current loops can flow along the field lines and terminate in sheaths (sheath-connected case), or in the opposite extreme, close locally by cross-field ion polarization drifts (disconnected). [3] In intermediate cases, current loop closure is facilitated at X-points by the flux tube fanning in divertor-type magnetic configurations. [4, 5] The physics 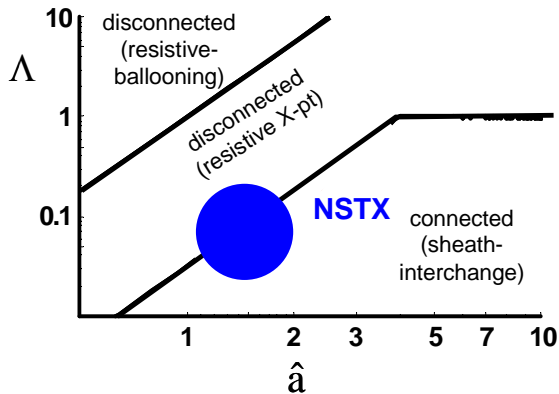of parallel disconnection can be simulated in 2D using a two-region electrostatic model which couples two planes ($\perp$ to B) by field line mapping and continuity equations for density and charge.[6] In particular, the current flow between regions is governed by the parallel plasma resistivity. Analytical analysis and numerical simulation confirm the existence of dimensionless blob regimes in this model, characterized by collisionality , $\Lambda = \nu_{ei}L_{\parallel}/\Omega_e\rho_s$ and dimensionless blob size $\hat{a} = a_b / a_* = a_b R^{1/5}/(L_{\parallel}^{2/5}\rho_s^{4/5})$. Here ν_{ei} is the collision frequency, $\Omega_j = eB/m_jc$ (j = e,i), $L_{\parallel}$ is the parallel magnetic connection length or blob parallel scale, a_b is the blob radius, and $\rho_s = c_s/\Omega_i$. A characteristic regime diagram is shown in Fig. 1. The precise location of the boundaries is influenced by the magnetic geometry, i.e. $\Lambda=\Lambda(\hat{a}, \varepsilon_x)$, where $\varepsilon_x < 1$ is a geometry parameter that approaches zero on the separatrix. Each blob regime has specific scalings of the blob radial velocity v_r that can be tested against experiments. The NSTX data described below is marginally in the connected sheath-interchange regime [1, 2] where $v_r = c_s q (\rho_s/a_b)^2$ and $q = L_{\parallel}/R$.

FIG. 1. Regimes of blob propagation

In general the blob radial velocity tends to increase with plasma collisionality Λ and has different dependencies on scale size $\hat{a}$ in each regime. The collisionality dependence is because curvature drift acts as a current source, and leads to larger potentials when the net circuit resistance is large. In terms of the characteristic velocity $v_* = c_s(a_*/R)^{1/2}$ the blob velocity is bounded in electrostatic theory by the inequalities

$$\frac{1}{\hat{a}^2} < \frac{v_r}{v_*} < \hat{a}^{1/2} \tag{1}$$

The minimum blob velocity ($1/\hat{a}^2$) occurs in the sheath-connected limit because in this case current is free to flow along the field lines and is regulated only by the sheath boundary condition, $J_{\parallel sh} \approx nec_s(e\Phi_{sh}/T)$. This situation provides the minimum circuit resistance, hence the minimum blob (dipole) potential and E×B speed for a given curvature drive (which provides a constant current source). In the opposite limit of high collisionality (resistive ballooning regime), parallel resistance impedes current flow to the sheaths, and instead the current loops are forced to close by ion polarization current across field lines. In this circumstance the circuit resistance, blob potential, and E×B speed are large. Numerical simulations of the propagation of individual blobs [6] confirms the collisionality dependence and different $\hat{a}$ dependences expressed in Eq. (1) for the low and high collisionality cases.

2.2 Modeling of Gas Puff Imaging (GPI) Experiments

The GPI technique consists of recording with high temporal and spatial resolution light generated by neutral atoms puffed into the edge of the plasma. Previous modeling [7] and analysis [8] have shown that the behavior of the neutral atoms does not cause the spatial characteristics of the observed emission patterns to deviate qualitatively from those of the underlying plasma turbulence. Here we first consider whether or not the single state, "collisional radiative" (CR) model of the helium atom to be used in the analysis of Sec. 2.3 provides adequate temporal resolution. In this model, the effects of all of the atom's excited states are folded into effective ionization and emission rates for the ground state, with the emission rate written as $S = n_0 F(n_e, T_e)$, where n_0 is the helium ground state density and the model provides the value of F for a given n_e and T_e. We have applied the analysis described in [9] to this model and find that for GPI-relevant parameters, this representation closely approximates the full system of equations describing the excited atomic states and that the model is able to resolve time scales longer than about 1 µs [10]. This is sufficient for present purposes since the GPI camera provides at best 4 µs resolution. Moreover, when we compare the emission expected from this model for time varying plasma parameters typical of GPI observations in NSTX, it matches very closely that obtained by integrating the full system of equations in time [10].

We can estimate the neutral density n_0 appearing in the expression for the emission rate S with steady state neutral transport simulations performed with the DEGAS 2 code [11]. As in [12], these simulations are fully 3-D, including the shape of the GPI gas manifold and emulation of the 64 by 64 pixel view of the GPI camera. We use calibration data to take into account the nonlinearity in the camera response and the vignetting of the optical system. The DEGAS 2 meshes are based on EFIT equilibria at the time of interest. We assume that $n_e=n_i$ and $T_e=T_i$ are constant on a flux surface and get the values of n_e and T_e at midplane from a single time Thomson scattering profile. We consider NSTX discharges 112811 (H-mode) and 112814 (L-mode) and compare the resulting 5876 Å image with the 25%, 50%, and 75% contours of the median average over the 300 frames recorded by the GPI camera [10]. The radial widths and peak locations of the observed and simulated emission clouds agree to within about 2 pixels (equivalent to 0.7 cm at the cloud location), less than the estimated uncertainties [10].
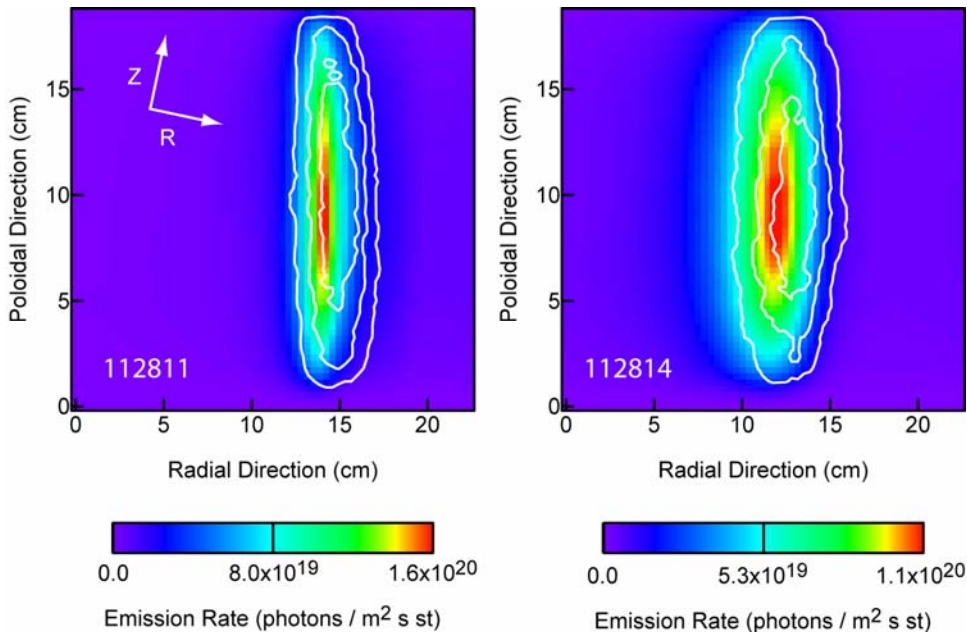

FIG. 2. Simulated (color images) and observed (line contours) camera data for NSTX shots 112811 and 112814.

2.3 Analysis of blob birth and transport from GPI Data

Analysis of GPI "movies" taken using a He gas puff in D plasma have been used to create a database of blob parameters: birth zone, blob scale size a_b, v_r and density and temperature. Measured properties were compared with theory for a small subset of bright, long-lived, isolated blobs for which relatively accurate v_r determinations could be made. We infer both the plasma density and temperature from the He 5876 emission via the CR model relationship $S = n_0 F(n_e, T_e)$ by postulating a relationship between n_e and T_e. Namely, in the blob paradigm, transport of the plasma occurs by convection (charge-separation-induced E×B drift). Consequently, we assume that the blobs convect density and temperature together over short distances from the blob birth zone (before parallel losses dominate). This results in the convect ansatz $T_e = T_e(n_e)$, employed in the analysis described here.

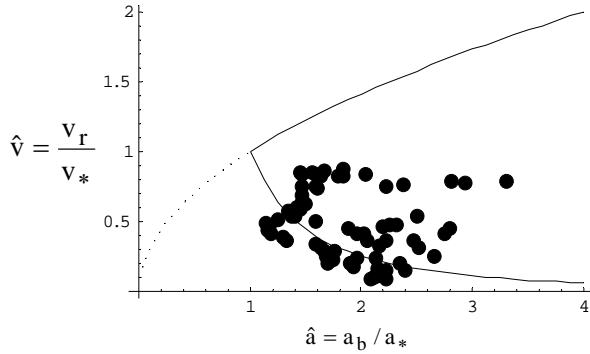$$\hat{v} = \frac{v_r}{v_*}$$

$$\hat{a} = a_b / a_*$$

FIG. 3. Observed radial blob velocities (filled circles) in dimensionless parameter space of velocity and blob scale size. The data is approximately bounded by a theoretically predicted minimum and maximum (solid lines).

For each blob in the dataset, the dimensionless parameters $\hat{a}$ and $\hat{v} = v_r / v_*$ were computed. Results are shown in Fig. 3. Here we estimate the blob parallel scale length (which is not directly measured) as $L_\parallel \sim qR$ using the local outboard $q \sim 1$ in NSTX. The solid lines in Fig. 2 for the region $\hat{a} > 1$ show the theoretical minimum and maximum bounds from Eq. (1). For $\hat{a} < 1$, the curve is a continuation of the maximum (resistive ballooning or inertial) scaling, however in this regime Kelvin Helmoltz blob instabilities should preclude long-lived coherent objects [13]. The NSTX blob data is seen to lie in approximately the expected range of $\hat{a}$ and roughly adheres to the expected theoretical bounds. As might be expected from Fig. 1, which suggest the observed blobs lie closer to the connected sheath-interchange regime than to the disconnected resistive ballooning regime, most of the blob data points lie closer to the lower bound. On the high side, the experimental points are bounded by $\hat{v} < 1$, independent of $\hat{a}$, which is suggestive of electromagnetic "high-beta" or "RX-EM" blob scaling [3, 4] where $v_{RXEM}/v_* \sim q^{4/5}\beta^{1/2}(R/\rho_s)^{2/5} \sim 0.2 - 1$ for this data with $\beta = c_s^2/v_a^2$. Increased blob speeds could be achieved if the more collisional regime (i.e. $\hat{v} \sim \hat{a}^{1/2}$) can be accessed, and this might provide an avenue for increasing the SOL width.

Additional analysis of this dataset (not shown here) was undertaken in an attempt to verify detailed v_r scaling laws for blobs in each regime. Scatter plots of the observed velocity vs. the theoretical velocity for the connected sheath-interchange limit again show that the expected bound is obeyed within error bars, but that the observed velocity can exceed the theoretical minimum velocity by a factor that depends on position and is qualitatively consistent with separatrix and partial parallel "disconnection" effects. Additional physics not in the present model also influences v_r.

Blob tracking and the inversion of the emission data to construct blob n_e and T_e can also be employed to deduce the "birth zone" of the blobs. Blob trajectories are propagated backward in time until the blob parameters match the n_e and T_e of the background profiles. This analysis shows that the blob birth zone is near the local maximum of the normalized edge pressure gradient $\nabla \, ln \, <p>$ suggesting blob generation by an underlying edge instability.

Further details of these results will be presented elsewhere.[14]

3. Accretion theory of spontaneous rotation

3.1 Experiments and theoretical developments (Coppi, Lontano, Varischetti)

Experiments – A new series of experiments showing spontaneous rotation, support key elements of accretion theory [15, 16]. This theory describes the flow of angular momentum, viz. ejection to the wall and transport (by both diffusion and an inflow velocity) to the core. [17] Key elements of the theory are: i) there is an intrinsic connection between thermal energy transport and spontaneous rotation [15, 16]; ii) rotation is strongly affected by the physical regime characterizing the edge plasma and the local magnetic configuration as the ejection of momentum to the wall is due to edge plasma modes; iii) rotation is inverted in the transition from the L-regime to a good ion confinement regime; iv) the phase velocities of the edge modes are inverted in this transition, as confirmed on JET [18].

In the H-regime, sharp edge density gradients imply stable ITG modes so momentum ejection is governed by unstable collisional ballooning modes [19] with phase velocities in the v_{de} direction, as seen on JET [20]. At the same time, in a flatter density core, ITG modes (v_{di} direction) carry angular momentum to the center of the column. A good indicator of this is that on Alcator C-Mod, when density peaking inhibits the ITG, v_ϕ does not reach the center. [21] The fact that the edge of the plasma column plays an important role has been demonstrated experimentally by changing the separatrix configuration from a lower to an upper null in Alcator C-Mod, observing a drastic change in the value of v_ϕ.
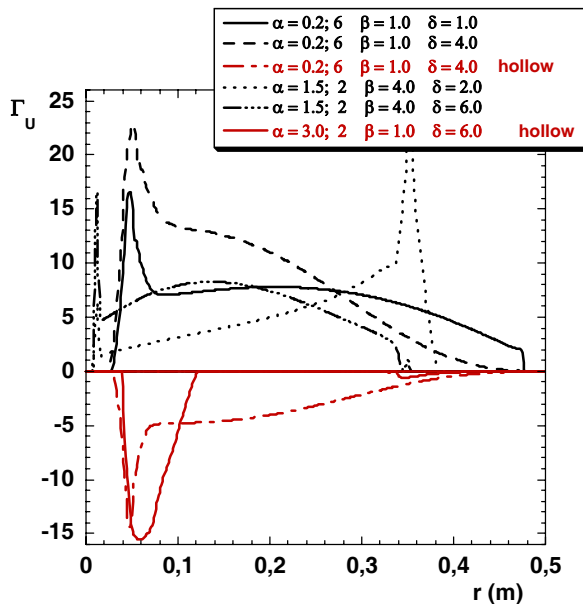

FIG. 4. Quasilinear radial momentum flux, for different plasma profiles Red curves refer to inverted (hollow) equilibrium ion flows.

ITG theory – In Fig. 4 the radial profiles of the quasi-linear longitudinal momentum flux $\Gamma_{v\parallel} = Mn_i < \tilde{v}_{Ex} \ \tilde{v}_\parallel >$ normalized to $n_iM(cT_e/eB)k_\perp c_s e^2|\tilde{\phi}|^2/T_e^2$ is given for different density (α-index), temperature (β) and equilibrium parallel ion velocity (δ) profiles. Low α-values correspond to very flat density profiles in the core plasma region. The negative fluxes ("hollow") appear when the equilibrium velocity is minimum on-axis. Here, $\tilde{v}_{Ex}$ and $\tilde{v}_\parallel$ are the perturbations of the electric drift velocity and of the parallel ion velocity, respectively. If the momentum source is localized at the edge, collisionless ITG-like modes are excited, that are able to transfer momentum inward: the flatter the density profile, the broader the radial extent of the region of excitation of such modes.

The model, which has been developed to study the linear ITG stability issue, is based on a two-fluid guiding center approximation, including the effects of the spatial variation of the magnetic field and of its curvature, by means of a gravitational-like drift velocity [22, 23]. As shown in Ref. 23, the presence of a sheared parallel velocity $U'_\parallel(r) < 0$ stabilizes the ITG modes (at high η_i-values), while a new unstable region at low values of both $|R/L_n|$ and $|R/L_T|$, rapidly increasing with $|U'_\parallel(r)|$, appears, which dominates the mode instability. We have verified that the presence of a sheared ion flow $U'_\parallel(r) \neq 0$ causes an asymmetric

excitation of ITG modes [15, 16, 27] and that the anomalous transport of momentum is produced by this spectral asymmetry in $k_\parallel$.

3.2 Blob, edge modes and momentum transport (Coppi, Lontano, Varischetti)

Blobs at the edge of the plasma column are assumed to emerge from the excitation of collisional ballooning modes that are driven by the combined effects of the plasma pressure gradient and the magnetic field curvature, and are allowed by the finite local resistivity. Under conditions that are characteristic of the H-regime, featuring a sharp density gradient (pedestal) at the edge and a considerable temperature, the instability found from the relevant dispersion relation corresponds to the well known resistive ballooning mode [19] with a phase velocity in the direction of the electron diamagnetic velocity. Conversely, when the temperature of the edge region is considerably lower than in the case of the H-regime, but the pressure gradient is significant, the same dispersion relation [24,25] including the effects of ion-ion collisions [24] indicates that the phase velocity can change sign. This is consistent with the accretion theory [15] and a parameter that may be used to distinguish the two regimes is $\mathcal{H} \equiv \omega_A^2/(\nu_{\mu\perp}D_m k^2)$ where $D_m = \eta c^2/(4\pi)$, η is the resistivity, $\nu_{\mu\perp} = D_{\mu\perp}k^2$ and $D_{\mu\perp}$ is the relevant transverse viscous diffusion coefficient. The relevant model dispersion relation is

$$(\omega + i\nu_{\mu\perp})(\omega - \omega_{di}) \approx \frac{\omega_A^2}{1 + iD_m k^2/(\omega - \omega_{*e}^T)} - \gamma_I^2, \tag{2}$$

where $\gamma_I^2 = (2/R_c)(-dp/dr)/\rho$, R_c is the local radius of magnetic field curvature, $\omega_A = k_\parallel v_A$, $\omega_{di} = k_\perp v_{di}$, $\omega_{*e}^T = -\omega_{di}(d\,ln\,p_e/d\,ln\,p_i) - \alpha_T k_\perp c(dT_e/dr)/(eB)$, $\alpha_T \approx 0.7$ and v_{di} is the ion diamagnetic velocity. The considered plane geometry mode is represented by the perturbed density $\hat{n} = \tilde{n}(x)exp(-i\omega t + ik_\perp y + ik_\parallel z)$ with $k_\perp^2 >> \partial^2/\partial x^2$.

The transport of the recoil momentum (directed as that of the ion diamagnetic velocity in the H-regime) toward the center of the plasma column is attributed to other modes that are traveling along the field and involve the effects of the gradients of both the ion flow velocity and temperature. These are called VTG modes which under stationary conditions, are purely oscillatory and produce a (quasi-linear) net flux of angular momentum that is null (the outward diffusion associated with the velocity gradient being compensated by the inward transport associated with the ion temperature gradient). The dispersion relation for the "primary" VTG mode is based on taking into account the contribution of both the quasi-linear transverse conductivity associated with the ion temperature gradient and the quasi-linear viscosity associated with the velocity gradient. The result, for the primary mode, is

$$\omega_0^2 + \omega_{Ti}\omega_0 \frac{k_\parallel^2 v_s^2}{\omega_0^2 + \nu_T^2} = -k_y k_\parallel D_B \frac{dV_\parallel}{dx}, \tag{3}$$

where $k_y k_\parallel dV_\parallel/dx < 0$, ω_0 is the mode frequency, $D_B \equiv cT_e/(eB)$, $\omega_{Ti} \equiv k_y c (dT_i/dx)/(eB)$, $v_s^2 = T_e/m_i$ and ν_T is the thermal diffusion rate. This is related to the viscous diffusion rate ν_μ by $\nu_T = \nu_\mu(\omega_0/\omega_{Ti})(\omega_0^2 + \nu_T^2)/(k_\parallel^2 v_s^2)$ where $\omega_0/\omega_{Ti} > 0$ indicating that the mode has a phase velocity in the direction of the ion diamagnetic velocity. The relevant momentum flux is proportional to

$$-\frac{\nu_\mu}{\nu_\mu^2 + \omega_0^2}\left(\frac{dV_\parallel}{dx} + \frac{k_\parallel}{m_i}\frac{dT_i}{dx}\frac{1 + \nu_T/\nu_\mu}{\omega_0^2 + \nu_T^2}\omega_0\right) \tag{4}$$

and vanishes when the dispersion relation (3) is satisfied. The primary mode ($k_y k_\parallel > 0$) is in fact driven unstable during the phase when the angular momentum propagates from the edge region toward the center of the plasma column as a result of $dV_\parallel/dx$ being positive combined with the effect of dT_i/dx. Clearly, this mode is turned off if $dV_\parallel/dx = 0$. The secondary mode

$(k_y k_\| < 0)$ can achieve a saturated state when $dV_\|/dx < 0$ if coupled non-linearly to the primary mode. Taking this into account an equation of the kind represented by Eq. (3) has been derived and the relevant quasi-linear flux of momentum has been shown to vanish.

In spite of the relatively large number of experiments that have shown evidence of the spontaneous rotation phenomenon, a scaling for the toroidal velocity that could represent the results by different machines has not been obtained. In fact, this may not be a fruitful undertaking as the toroidal velocity can acquire different profiles (e.g. peaked, flat, with a "central hole") and is influenced by details of the regimes of both the edge and central region of the plasma column.

3.3 Nonlinear edge plasma simulations

Here, we numerically solve a 2D model similar to the Wakatani-Hasegawa [26] and blob models [1, 2]. Employing the momentum conservation law, we derive a y-averaged (y ≈ poloidal) equation to account for momentum flow across the last closed surface.

$$\frac{\partial}{\partial t}\langle n v_y \rangle + \frac{\partial}{\partial x}\langle n v_x v_y \rangle = \int_{x_{LCS}}^{x} dx\, \alpha_{sh}\langle n\Phi \rangle \qquad (5)$$

where the RHS accounts for momentum loss to the sheaths in the SOL through the sheath current $J_\| \sim \alpha_{sh}\Phi$.

Results are shown in Fig. 5. Blob ejection events occur at the spikes in radial particle flux $\Gamma = \langle nv_x \rangle$ and momentum flux $\langle nv_x n_y \rangle$. The sign of the ejected blob momentum is correlated with the sign of $\langle v_y \rangle'$ at the time of blob ejection. Blobs carry net momentum to the sheaths and the net back reaction spins up the momentum of the core plasma, as shown in the top panel. Quasilinear calculations on this nonlocal system using a radial eigenvalue code show that $\langle nv_x n_y \rangle / \langle nv_x \rangle$ is a function of $\langle v_y \rangle'$ and changes sign at large positive $\langle v_y \rangle'$ as also seen intermittently in Fig. 5.

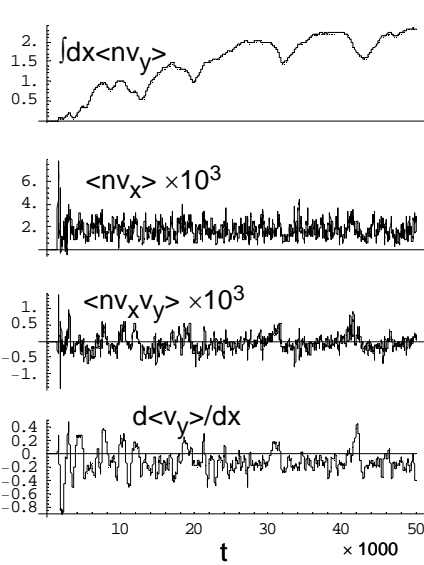*FIG. 5. Edge turbulence simulation results showing time histories of net core momentum, $\langle nv_x \rangle$, $\langle nv_x v_y \rangle$, and $\langle v_y \rangle'$ (just inside the LCS).*

The E×B drifts in the binormal (y) direction drive poloidal flows and additionally have a small toroidal projection. However, toroidal flows are also driven by the radial flux of parallel momentum $\langle nv_x n_\| \rangle$. The preceding QL radial eigenvalue model is easily extended to investigate this in the limit $\omega > k_\| c_s$ where sound wave coupling can be neglected in the basic drift-curvature equations that govern the Wakatani-Hasegawa and blob equations. The linearized parallel velocity response $\tilde{v}_\|$ is obtained from the parallel momentum equation, $-i\hat{\omega}\tilde{v}_\| = -\tilde{v}_x \bar{v}_\|' - c_s^2 \nabla_\|\tilde{n}/n$ where $\hat{\omega} \equiv \omega - k_y\bar{v}_y' x - k_\|\bar{v}_\|' x$ and $' = \partial/\partial x$. This yields

$$\langle n v_x v_\| \rangle \approx \bar{n}\langle \tilde{v}_x \tilde{v}_\| \rangle + \bar{v}_\|\langle \tilde{n}\tilde{v}_x \rangle = -D\bar{n}\frac{\partial \bar{v}_\|}{\partial x} + \left(\bar{v}_\| + \frac{c_s^2 k_\|}{\hat{\omega}} \right)\langle \tilde{n}\tilde{v}_x \rangle \qquad (6)$$

Here $D = \gamma \langle (\tilde{v}_x/\hat{\omega})^2 \rangle$ is the quasilinear diffusion coefficient, and the terms proportional to the particle flux $\langle nv_x \rangle$ give a momentum pinch. In particular, the term proportional to $k_\|/\hat{\omega}$ represents the parallel wave momentum carried outward by the blobs.

Analogous to the ITG mode studies mentioned in Sec. 3.1 and in Ref. 27, the spectral asymmetry in $k_\|$ required for a net toroidal force can arise from the sheared flow $\bar{v}_\|'$ itself.

Indeed, the linear growth rate for the drift-curvature modes in the present model peaks at $k_\parallel \neq 0$ when $\overline{v}_\parallel' \neq 0$.

[1]   KRASHENINNIKOV, S.I., Phys. Letters A **283**, 368 (2001).
[2]   D'IPPOLITO, D.A., MYRA, J.R. and KRASHENINNIKOV, S.I., Phys. Plasmas **9**, 222 (2002).
[3]   MYRA, J.R. and D'IPPOLITO, D.A., Phys. Plasmas **12**, 092511 (2005).
[4]   KRASHENINNIKOV, S.I., ,RYUTOV, D.D., and YU, G.Q., J. Plasma Fus. Res. **6**, 139 (2005).
[5]   RUSSELL, D.A., D'IPPOLITO, D.A., MYRA, J.R., NEVINS, W.M. and XU, X.Q., Phys. Rev. Lett. **93**, 265001 (2004).
[6]   MYRA, J.R., RUSSELL, D.A. and D'IPPOLITO, D.A., Lodestar Report #LRC-06-111 (2006), to be published in Phys. Plasmas.
[7]   STOTLER, D.P. et al., J. Nucl. Mater. **313-316**, 1066 (2003).
[8]   ZWEBEN, S.J. et al., Nucl. Fusion **44**, 134 (2004).
[9]   GREENLAND, P.T., J. Nucl. Mater. **290-293**, 615 (2001).
[10]   STOTLER, D.P. et al., J. Nucl. Mater. (to be published).
[11]   STOTLER, D.P. and KARNEY, C.F.F., Contrib. Plasma Phys. **34**, 392 (1994).
[12]   STOTLER, D.P. et al., Contrib. Plasma Phys. **44**, 294 (2004).
[13]   YU, G. Q. and KRASHENINNIKOV, S. I., Phys. Plasmas **10**, 4413 (2003).
[14]   MYRA, J.R., D'IPPOLITO, D.A., STOTLER, D.P., ZWEBEN, S.J., et al., Lodestar Report #LRC-06-110 (2006), to be published in Phys. Plasmas.
[15]   COPPI, B., Nucl. Fusion **42**, 1 (2002).
[16]   COPPI, B., Paper IAEA-CN-94-TH/P1-02, 19th IAEA Fusion Energy Conference (Lyon, France, 2002).
[17]   COPPI, B., PENN, G., SUGIYAMA, L.E., Paper IAEA-F1-CN-TH3/7, 17th IAEA Fusion Energy Conference (Yokohama, Japan, 1998).
[18]   FASOLI, A. and SHARAPOV, A., private communication (2002), to be published.
[19]   COPPI, B., ROSENBLUTH, M.N., Plasma Phys. Cont. Fus. Res. **1**, 617 (IAEA, Vienna, 1966).
[20]   SMEULDERS, P., CONWAY, G.D., ALPER, B., et al., Plasma Phys. Cont. Fus. **41**, 1303 (1999).
[21]   MARMAR, E.S., BAI, B., BOIVIN, R.L., et al., Paper IAEA-CN-94-OV/4-1, 19th IAEA Fusion Energy Conference (Lyon, France, 2002).
[22]   COPPI, B., VARISCHETTI, M.C., LAZZARO, E., and LONTANO, M., Proc. 33rd E.P.S. Conf., London, 2006, P-5.079 (2006).
[23]   LONTANO, M., VARISCHETTI, M.C., and LAZZARO, E., Proc. Joint Varenna-Lausanne Int. Workshop, AIP Proceeding Series, in press (2006).
[24]   COPPI, B., M.I.T. – L.N.S. Report H.E.P. 06/01 (April 2006), Invited Paper, I.T.P.A. Meeting, Princeton, N.J.
[25]   COPPI, B. D'IPPOLITO, D., KRASHENINNIKOV, S.I., et. al. Proc. 33rd E.P.S. Conf., Rome, 2006, Paper O4.017 (2006)
[26]   WAKATANI, M. and HASEGAWA, A., Phys. Fluids **27**, 611 (1984).
[27]   COPPI, B., LAZZARO, E., LONTANO, M. and MARCHETTO, C., Proc. 31st E.P.S. Conf., London, 2004, Vol.28G, P-2.120 (2004).